



UNIVERSITY OF LEEDS

This is a repository copy of *The effect of the ratio of solid to liquid conductivity on the side-branching characteristics of dendrites within a phase-field model of solidification*.

White Rose Research Online URL for this paper:
<http://eprints.whiterose.ac.uk/84396/>

Version: Accepted Version

Article:

Mullis, AM (2006) The effect of the ratio of solid to liquid conductivity on the side-branching characteristics of dendrites within a phase-field model of solidification. *Computational Materials Science*, 38 (2). 426 - 431. ISSN 0927-0256

<https://doi.org/10.1016/j.commatsci.2006.03.010>

© 2006, Elsevier. Licensed under the Creative Commons Attribution-NonCommercial-NoDerivatives 4.0 International
<http://creativecommons.org/licenses/by-nc-nd/4.0/>

Reuse

Unless indicated otherwise, fulltext items are protected by copyright with all rights reserved. The copyright exception in section 29 of the Copyright, Designs and Patents Act 1988 allows the making of a single copy solely for the purpose of non-commercial research or private study within the limits of fair dealing. The publisher or other rights-holder may allow further reproduction and re-use of this version - refer to the White Rose Research Online record for this item. Where records identify the publisher as the copyright holder, users can verify any specific terms of use on the publisher's website.

Takedown

If you consider content in White Rose Research Online to be in breach of UK law, please notify us by emailing eprints@whiterose.ac.uk including the URL of the record and the reason for the withdrawal request.



eprints@whiterose.ac.uk
<https://eprints.whiterose.ac.uk/>

The Effect of the Ratio of Solid to Liquid Conductivity on the Sidebranching Characteristics of Dendrites within a Phase-field model of Solidification.

A. M. Mullis

Institute for Materials Research, University of Leeds, Leeds LS2 9JT, UK

ABSTRACT

We use a phase-field model of dendritic growth in a pure undercooled melt to examine the effect of the ratio of the thermal conductivities in the solid and liquid states ($\mu = \kappa_s/\kappa_l$) on the side-branching characteristics of the dendrite. We find that high conductivity in the solid favours extensive side-branching while low conductivity in the solid appears to strongly suppress side branching. Over the range $0.5 \leq \mu \leq 2.0$, which is typical of most (metallic) systems which display dendritic growth the RMS distance at which the mean amplitude of the side-branches becomes equal to the tip radius varies from as little as 10 tip radii to in excess of 45 tip radii. This implies that there may be significant morphological difference between dendrites grown in different materials. The variation does not appear to follow exactly the analytical relationship predicted by solvability theory.

PACS: 81.30.Fb, 64.70.Dv, 82.20.Wt

Keywords: rapid solidification, phase-field models

1. Introduction

One of the most fundamental and all pervasive microstructures produced during the solidification of metals is the dendrite. The dendrite is a prime example of a pattern forming system where complex morphologies arise from initially homogeneous conditions due to the highly non-linear response of the controlling system.

In recent years the theory of microscopic solvability [1, 2] has provided a plausible explanation for many of the features of dendritic growth at both low and arbitrarily high undercoolings including selection of the operating point of the needle crystal, R , the shape of the tip region and the formation of the side-branch structures [3, 4, 5]. The principal prediction of solvability theory is that the anisotropy of the capillary forces break the Ivantsov [6] degeneracy found in isotropic models via the relationship

$$R^2V = \frac{2ad_o}{\sigma^*} \quad (1)$$

where R is the radius of curvature at the tip, V is the growth velocity and d_o is the thermal capillary length, defined by

$$d_o = \frac{\sigma T_m c}{L^2} . \quad (2)$$

Here L is the latent heat per unit volume, c the specific heat per unit volume, σ the interfacial energy between the solid and liquid phases, T_m the melting temperature, γ_d is the strength of the capillary anisotropy and a is the thermal diffusivity. σ^* is the anisotropy dependant eigenvalue for the problem, which for small Peclet numbers and

in the limit of vanishing anisotropy is found to vary as $\sigma^*(\gamma) \propto \gamma_d^{7/4}$, where the Peclet number is defined as

$$p = \frac{VR}{2a} \quad (3)$$

and anisotropy has been introduced by letting

$$d_o \rightarrow d_o(\theta) = d_o(1 - \gamma_d \cos k\theta) \quad (4)$$

where θ is the angle between the local outward pointing normal to the interface and the principal growth direction and k is a mode number, which for growth in a cubic metal will be 4.

Further progress has been made towards understanding dendritic growth, particularly the time-dependant problem, by the advent of phase-field modeling [7, 8]. The basis of the phase-field technique is the definition of a phase variable, $\phi(\mathbf{x}, t)$, which is continuous over the whole domain Ω occupied by the system, where the continuity of ϕ over Ω implies that the interface between the solid and liquid regions is diffuse. The evolution of the phase variable, ϕ , is governed by a free energy functional which ensures an increase in entropy with time.

Imaging of dendritic growth in transparent analogue casting systems, such as succinonitrile [9] and xenon [10], show that close to the tip region the dendrite is free from side-branching. Moving away from the tip small oscillations are initiated which grow as they move down the dendrite trunk. Initially the spacing of these perturbations

is uniform. However, as amplification of the initial perturbations proceeds the process becomes competitive with faster growing side-arms becoming dominant, leading to a less uniform spacing. Eventually coarsening becomes dominant, with side-arms of higher curvature being preferentially re-melted [11, 12].

A number of measures have been proposed to quantify the side-branch morphology of dendritic structures. The simplest, and often the only measure that can be applied to as-solidified materials, is the secondary arm spacing, λ_2 . However, when the growing dendrite can be imaged *in situ* a far greater range of measures may be applied. The most direct is \bar{z}_{sb} , which is the mean distance along the trunk (in units of R) at which the amplitude of the side-branching becomes equal to R . Other measures which have been used in the literature [10, 13] to characterise dendritic structures include the fractal dimension, shape parameterization of the inner and outer side-branch envelopes, projection area and contour length.

Probably the most carefully controlled study of dendritic growth to be undertaken is the Isothermal Dendrite Growth Experiment [14] (IDGE), in which the onset of side-branching, as measured by the distance to the first detectable side-branch, was determined for high purity succinonitrile under microgravity conditions. This was determined as being at $(11.8 \pm 1.7)R$. In a control experiment, which was identical except that it was performed under terrestrial gravity, the same measurement yielded $(12.7 \pm 2.3)R$. Bisang & Bilgram [10] have measured \bar{z}_{sb} for xenon dendrites under terrestrial conditions, finding $\bar{z}_{sb} = (17.5 \pm 3)$. This figure is somewhat higher than that found during IDGE due to the different methodologies applied, the first detectable side-

branch having an amplitude significantly less than $1R$, so that the two data sets are probably mutually consistent.

Models of side-branch development within the theory of microscopic solvability have been put forward by Langer [3, 4] and by Brener & Tempkin [5]. These models propose that side-branches grow due to the selective amplification of thermally induced noise at the solid-liquid interface. For axi-symmetric dendrites Langer proposed that side-branches would grow such that :

$$\bar{z}_{\text{sb}} = \frac{(\sigma^*)^2}{2} \left(\frac{3}{2}\right)^6 \ln^4(\bar{S} \bar{C}) \quad (5)$$

where \bar{C} is a constant of order unity and \bar{S} is the strength of the thermal noise,

$$\bar{S} = \left(\frac{T}{T_o}\right) (\sigma^*)^{3/2} p \quad (6)$$

where

$$T_o = \left(\frac{L^2 d_o^3}{k_B c}\right)^{\frac{1}{2}} \quad (7)$$

and k_B is the Boltzmann constant. For succinonitrile at low undercooling, Langer found that $\bar{C} = 10^2 - 10^3$ was required to reproduce the experimentally observed level of side-branching.

However, due to their complexity, solvability models are often restricted to the assumption of either symmetric or asymmetric conductivity, that is either $\kappa_s = \kappa_l$ or

$\kappa_s = 0$, where κ_s and κ_l are the thermal conductivities of the solid and liquid phases respectively. The effect of non-symmetric conductivities in microscopic solvability has been investigated to first order by Barbieri & Langer [15] who find the

$$\sigma^*(\mu) \approx \frac{2}{1+\mu} \sigma^*(\mu=1) \quad (8)$$

where $\mu = \kappa_s/\kappa_l$. Phase-field method have also recently been used to study the effect of non-symmetric thermal conductivities on σ^* [16]. This study found that although the relationship of Barbieri & Langer was recovered in the limit of vanishing Peclet number ($p \rightarrow 0$), significant departures would be encountered for finite p , particularly for the case $\mu < 1$.

In this paper we use a phase-field model of dendritic growth in a pure undercooled melt to probe the effect of the ratio μ on side-branch formation.

Although $\kappa_s = \kappa_l$ is a common assumption in the modelling of thermal dendritic growth, reduced phonon scattering in the solid phase, relative to the liquid, means that in reality $\kappa_s > \kappa_l$ most metallic materials. However, quantifying the ratio κ_s/κ_l , even for pure metals, is difficult due to the scarcity of thermal conductivity data for liquid metals. For solid metals at high temperature the Wiedemann-Franz-Lorenz law,

$$\frac{\kappa}{\sigma_e T} = \frac{\pi^2 k_B^2}{3e^2} = 2.45 \times 10^{-8} \text{ W } \Omega \text{ K}^{-1} \quad (9)$$

is generally a reasonable approximation for all metals, where σ_e is the electrical conductivity. A number of studies [17, 18] have shown that this relationship also appears to hold for liquid metals, and consequently the ratio σ_{es}/σ_{el} may be used as a guide to κ_s/κ_l . This ratio is typically around 1.5 for many metals although the variations are quite large. Values as low as 1.05 have been reported for Fe [19, 20] while Cu, Ag and Au all have values [21] close to 2. Mn is exceptional for a metal in that $\sigma_{es}/\sigma_{el} = 0.6$ [21]. Si and Ge show $\sigma_{es}/\sigma_{el} \ll 1$, although as this is due to the phase change from a semi-conducting solid to a metallic liquid, electrical conductivity is probably not a good guide to thermal conductivity in these cases. Although both Si and Ge show faceted growth under conventional solidification conditions, Ge has been shown [22, 23] to grow dendritically during rapid solidification due to kinetic roughening of the solid-liquid interface [23]. On balance, we believe the range $0.5 \leq \kappa_s/\kappa_l \leq 2.0$ probably cover most materials of interest.

2. Computational Method

The basis of the Wheeler model is a Landau-Ginzberg free energy functional

$$F = \int_{\Omega} \left[s(e, \phi) + \frac{1}{2} \varepsilon^2 (\nabla \phi)^2 \right] d\Omega \quad (10)$$

where $s(e, \phi)$ is an entropy density, e is the internal energy density and ε is a constant. Here, $\phi \equiv 1$ in the liquid and 0 in the solid. Following Wheeler *et al.* [8] we define reference length and time scales w and w^2/D , and a dimensionless temperature u ($T = T_m + u\Delta T$) giving the transport equation as

$$\frac{\partial u}{\partial \tau} + \frac{30\phi^2}{\Delta}(1 - 2\phi + \phi^2) \frac{\partial \phi}{\partial \tau} = \nabla \cdot (\bar{a} \nabla u) \quad (11)$$

where \bar{a} is the thermal diffusivity of the material normalised to the value of that for the pure liquid, namely

$$\bar{a} = \frac{\phi a_1 + (1 - \phi) a_s}{a_1} \quad (12)$$

a_1 and a_s being the thermal diffusivities in the liquid and solid states respectively and Δ is the dimensionless undercooling

$$\Delta = \frac{c\Delta T}{L} \quad (13)$$

The second term on the left hand side of Equation (11) thus represents the latent heat associated with the change of state.

The anisotropic phase equation is given by

$$\begin{aligned} \frac{\bar{\varepsilon}^2}{m} \frac{\partial \phi}{\partial \tau} = & \phi(1 - \phi) \left[\phi - \frac{1}{2} + 30\bar{\varepsilon}\alpha\Delta u\phi(1 - \phi) \right] - \bar{\varepsilon}^2 \frac{\partial}{\partial x} \left(\eta(\theta)\eta'(\theta) \frac{\partial \phi}{\partial y} \right) \\ & + \bar{\varepsilon}^2 \frac{\partial}{\partial y} \left(\eta(\theta)\eta'(\theta) \frac{\partial \phi}{\partial x} \right) + \bar{\varepsilon}^2 \nabla \cdot (\eta^2(\theta) \nabla \phi) \end{aligned} \quad (14)$$

where the quantities in Equation (14) are given by Wheeler *et al.* [8] as

$$\alpha = \frac{\sqrt{2}wL^2}{12c\sigma T_m} \quad (15)$$

$$m = \frac{\xi \sigma T_m}{a_1 L} \quad (16)$$

and

$$\tilde{\varepsilon} = \frac{\delta}{w}. \quad (17)$$

Here δ is a parameter defining the width of the diffuse interface and ξ is the kinetic parameter.

The system of differential equations represented by Equations (11) and (14) is solved using a standard finite difference scheme. The transport equation is solved using an alternating direct implicit (ADI) scheme, which is unconditionally stable, irrespective of the time step, δt , employed. However, the phase field equation is highly non-linear, and consequently there is no simple implicit scheme suitable for its solution. We have therefore used an explicit numerical scheme to obtain the time-dependant solution to Equation (14). This will be subject to a Courant type stability condition of the form :

$$\delta t \leq \frac{(\delta x)^2}{\psi m} \quad (18)$$

where ψ would take the value 4 for a linear equation. The nonlinear nature of Equation (14) actually imposes a more restrictive condition on the time step and the optimum value of ψ has been determined empirically.

It can be shown that [8, 24] in the asymptotic sharp interface limit, $\tilde{\varepsilon} \rightarrow 0$, the interface temperature is given by

$$u = -\bar{d}_o \left(\frac{\bar{v}_n}{m[\eta(\theta)]^2} + [\eta(\theta) + \eta''(\theta)]\mathcal{K} \right) \quad (19)$$

where

$$\bar{d}_o = d_o \frac{L}{wc\Delta T} = \frac{\sigma T_m}{wL\Delta T} \quad (20)$$

is the dimensionless capillary length, \bar{v}_n is the dimensionless interface velocity along the outward pointing normal and \mathcal{K} is the interface curvature. By comparing Equation (19) with the standard expression for the interface temperature, T_i , of a solid growing into its parent liquid (see for instance Brener & Mel'nikov [25], Equ. 2.3) with anisotropic attachment kinetics of strength γ_k , it is clear that by introducing an anisotropy in the interface width the Wheeler model includes both capillary and kinetic anisotropy effects with a fixed ratio of capillary to kinetic anisotropy given by $\gamma_d/\gamma_k = (k^2-1)/2 = 15/2$ (for $k = 4$).

During the simulation the curvature, $1/R$, of the dendrite tip is evaluated along the x -axis (where the proscribed anisotropy ensures that the dendrite tip does grow along the x -axis). Following Wheeler [8] this may be written as

$$\frac{1}{R} = \frac{\phi_{yy}}{\phi_x} \quad (21)$$

The evolution of R is tracked to ensure that a steady state has been obtained for the grid on which the problem is running and once this is the case, a representative value R for the simulation is calculate by averaging over a minimum of 5000 time steps. Moreover,

for each set of material parameters (μ, p) each simulation is run a minimum of 4 times on successively finer grids to check that the numerical solutions are converging to give steady values of V and R . Initial simulations are conducted on a relatively coarse grid in which the grid spacing is set at approximately $R/20$, with each successive refinement of the grid being by a factor of $\sqrt{2}$.

Noise is introduced by modifying Equation (14) such that :

$$\frac{\bar{\varepsilon}^2}{m} \frac{\partial \phi}{\partial \tau} \rightarrow \frac{\bar{\varepsilon}^2}{m} \frac{\partial \phi}{\partial \tau} + 16\phi^2(1-\phi)^2 \mathfrak{R} \zeta_R \Theta \quad (22)$$

where \mathfrak{R} is a sample from a Gaussian distribution of random numbers with zero mean and unit variance, ζ_R is a constant determining the level of random noise and

$$\Theta = 30\bar{\varepsilon}\alpha\Delta u\phi^2(1-\phi)^2 \quad (23)$$

is just the first term from the right hand side of Equation (14). The term $16\phi^2(1-\phi)^2$ ensures that the introduced noise is confined effectively to the solid-liquid interface region. The value of the noise amplitude parameter, ζ_R , is set such that \bar{z}_{sb} takes values close to those found experimentally in transparent analogue systems for the case $\kappa_s = \kappa_l$. This procedure should thus allow a relatively reliable estimate of the relative variation of \bar{z}_{sb} with μ .

3. Results & Discussion

We have used \bar{z}_{sb} as the prime measure of the extent of side-branching displayed by the computed dendrite morphologies generated by our phase-field model. Consequently,

the variation of \bar{z}_{sb} with μ has been used to quantify the effect of μ on the morphology of the dendrites.

A typical dendrite geometry from our simulations is shown in Fig. 1, the material parameters used have been adopted from [16]. The same parameters have been used in all the simulations reported here except that κ_s has been varied to obtain the required value of μ (at fixed κ_l). This particular dendrite was grown at a Peclet number of $p = 0.1$. Also shown are the measurements made to determine the amplitude of a given side-branch. The amplitude, A_n , and lateral distance from the tip, Z_n , of each of the n visible side-branches is measured in units of R . With regard to the amplitude this is measured with respect to both the leading and trailing interdendritic depression (A and A' on Fig. 1) and an average value, \bar{A} is taken. \bar{z}_{sb} is determined by plotting \bar{A} against Z for all visible side-branches and determining the intercept of the best-fit line with $\bar{A} = 1$ (in units of R). However, during this calculation side-branches that have undergone obvious remelting during competitive growth (e.g side-branch $n = 7$, in Fig. 1) are removed from the data set.

The effect of varying μ on \bar{z}_{sb} has been studied over a wide range of growth velocities. Three typical sets of simulation data, corresponding to Peclet numbers of 0.05, 0.1 and 0.15, are shown in Fig. 2. As there is gradual decrease in \bar{z}_{sb} (side branches move closer to the tip) as the growth velocity increases, and in order to facilitate easy comparison of the data sets, we have in each case normalised against the value of \bar{z}_{sb} at $\mu = 1$, that is we have plotted $\bar{z}_n = \bar{z}_{sb}(\mu) / \bar{z}_{sb}(\mu = 1)$. This dependence of \bar{z}_{sb} on the

growth velocity is both predicted theoretically by Equation (5) and has been observed experimentally in a sequence of photographs of dendritic growth in succinonitrile by Huang & Glicksman [26].

Two main features of the data are apparent from Fig. 2. Firstly, it is clear that μ does indeed have a significant effect on \bar{z}_{sb} . On increasing μ from 1 to 2, \bar{z}_n drops initially quite rapidly before apparently levelling off around a value of 0.5. Conversely, on decreasing μ from 1 to 0.5, \bar{z}_{sb} increases to ≈ 2 , with no indication that the increase would level off if μ were decreased further. However, the effect of reducing μ below 0.5 has not been investigated because, as mentioned above, there are very few systems for which this combination of material parameters is likely to hold. Secondly, we notice that there is a very close correspondence between the three data sets despite their very different growth regimes. Indeed, to within the error associated with measuring \bar{z}_n from contour maps of $\phi = 0.5$ it is consistent that the three data sets display the same trend. Error bars have not been included on this figure as, with multiple data sets having the same value of the ordinate, the figure becomes difficult to read.

The corresponding variation in σ^* as a function of μ has been investigated in [16], where it was found that although the variation was in the same sense as that predicted by Barbieri & Langer [15] in the limit of vanishing kinetics, namely that σ^* varies as $2/(1+\mu)$, the magnitude of the variation was significantly greater. As, according to Equ. (5), there is a predicted variation of \bar{z}_{sb} with σ^* , namely $\bar{z}_{sb} \propto (\sigma^*)^2$, the general form of the variation reported in Fig. 2 might not appear unsurprising. However,

quantitatively the variation seen in our data is not just a manifestation of the relationship described by Barbieri & Langer. In particular two curves are also shown in Fig. 2. The dashed line is the predicted variation of \bar{z}_n when the corresponding measured values of σ^* (for $p = 0.1$) are substituted into Equ. (5). Clearly, the measured variation of \bar{z}_n with μ is much gentler than would be expected from Equ. (5). Infact, we find [Fig. 2, solid line] that to a very good approximation \bar{z}_n varies as $\{2/(1+\mu)\}^2$ irrespective of p , even though the $2/(1+\mu)$ scaling only appears to hold for σ^* at very low p .

The physical processes giving rise to this result are far from clear and here we offer no more than some preliminary speculation on the results. One of the primary differences between the solvability and phase-field formulations of the dendritic growth problem is that, on the whole, kinetic effects tend to be absent from solvability models, whereas the inclusion of anisotropic kinetics are implicit within the phase-field formulation of the problem. While solvability models have been formulated which contain kinetic effects [25], this was not the case in the models of Langer and co-workers [3, 4, 15] used to study the effects of μ on σ^* or to develop the theory of dendritic side-branching via the amplification of thermal noise. Consequently, these models are only strictly valid in the limit of vanishing Peclet number. It is, however, well established [25] that the kinetic anisotropy plays a role in the selection of the operating point parameter, σ^* . Indeed, it has been shown that the kinetic anisotropy is sufficient for growth of dendrites, even in the absence of a surface energy anisotropy. Moreover, if the directions of the kinetic and surface energy anisotropies do not coincide it has been shown that as the undercooling is increased the dendrite will switch directions from that favoured by the surface energy anisotropy to that favoured by the kinetic anisotropy [27, 28, 29].

The results of Mullis [16] show that the extent to which the variation of σ^* with μ departs from the predictions of solvability theory increases rapidly with increasing Peclet number. This would suggest that there is a strong kinetic effect present in the selection of σ^* at high p . Conversely, the results presented here indicate that \bar{z}_{sb} varies as $1/(1+\mu)^2$, which is as would be expected from solvability theory in the limit of vanishing Peclet number, even though the simulations here were run at $p = 0.1$. This would tend to suggest that, at least with respect to the variation of μ , kinetics play no part in determining the extent of dendritic side-branching.

4. References

1. D.A. Kessler, J. Koplik & H. Levine, *Adv. Phys.* **37** (1988), 255.
2. M. Ben-Amar & Y. Pomeau, *Europhys. Lett.* **2** (1986) 307.
3. M.N. Barber, A. Barbieri & J.S. Langer, *Phys Rev. A* **36** (1987), 3340.
4. J.S. Langer, *Phys. Rev. A* **36** (1987), 3350.
5. E. Brener & D. Temkin, *Phys. Rev. E* **51** (1995), 351.
6. G.P. Ivantsov, *Doklady Akademii Nauk SSSR* **58** (1947) 567
7. R. Kobayashi, *Physica D* **63** (1993) 410.
8. A.A. Wheeler, B.T. Murray & R.J. Schaefer, *Physica D* **66** (1993), 243.
9. D.P. Corrigan, M.B. Koss, J.C. La Combe, K.D. DeJager, L.A. Tennenhouse & M.E. Glicksman, *Phys. Rev. E* **60** (1999) 7217.
10. U. Bisang & J.H. Bilgram, *Phys. Rev. E* **54** (1996) 5309.
11. T.Z. Kattamis, J.C. Coughin & M.C. Flemings, *Trans. Met. Soc. AIME* **239** (1967), 1504.
12. K.P. Young & D.H. Kirkwood, *Met. Trans.* **6A** (1975), 197.

13. Q. Li & C. Beckermann, *Phys. Rev. E* **57** (1998) 3176.
14. L.A. Tennerhouse, M.B. Koss, J.C. LaCombe & M.E. Glicksman, *J. Cryst. Growth* **174** (1997) 82.
15. A. Barbieri & J.S. Langer, *Phys. Rev. A*, **39** (1989) 5314.
16. A.M. Mullis, *Phys. Rev. E*. **68** (2003) 011602.
17. G. Busch, H.-J. Güntherodt, W. Haller & P. Wyssmann, *Phys. Lett.* **43A** (1973) 225.
18. W. Haller, H.-J. Güntherodt & G. Busch, in ‘*Liquid Metals 1976*’, pp. 207, Institute of Physics Conference Series No. 30, Bristol, 1977.
19. Y. Ono & T. Yagi, *Trans ISIJ* **12** (1972) 314.
20. Y. Kita, M. Zeze & Z. Morita, *Trans ISIJ* **22** (1982) 571.
21. T. Iida & R.I.L. Guthrie, ‘*The Physical Properties of Liquid Metals*’, Clarendon Press, Oxford, 1988.
22. S.E. Battersby, R.F. Cochrane & A.M. Mullis, *Mater. Sci. Eng. A* **226** (1997) 443.
23. S.E. Battersby, R.F. Cochrane & A.M. Mullis, *J. Mater. Sci.* **34** (1999) 2049.
24. G.B. McFadden, A.A. Wheeler, R.J. Braun, S.R. Coriell & R.F. Sekerka, *Phys. Rev. E* **48** (1993) 2016.
25. E.A. Brener & V.I. Mel’nikov, *Adv. Phys.* **40** (1991) 53.
26. S.-C Huang & M.E. Glicksman, *Acta Metall.* **29** (1981) 717-734.
27. E. Ben-Jacob, P. Garik & D. Grier, *Superlattices Microstruct.* **3** (1987) 599.
28. T. Ihle, *Eur. Phys. J. B* **16** (2000) 337.
29. A.M. Mullis, *Europhys. J. B* **41** (2004) 377.

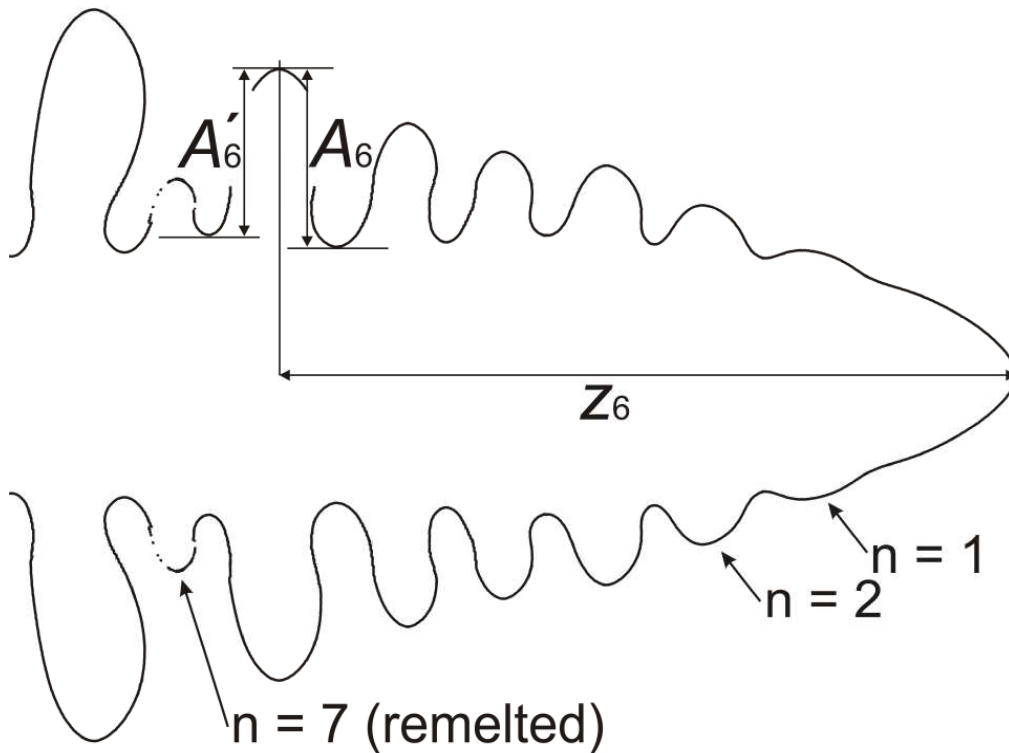


Figure 1. Typical dendrite morphology as generated by our phase-field simulation, showing here the first 8 detectable side-branches ($n = 1-8$). Also shown are the basic quantities used to determine \bar{z}_{sb} . These are the side-branch amplitude, A_n & A'_n (measured with respect to both the leading and trailing interdendritic troughs) and the lateral distance from the tip, Z_n . For illustration purpose these are just indicated for $n = 6$, but would actually be measured for all visible side-branches.

Fig. 2

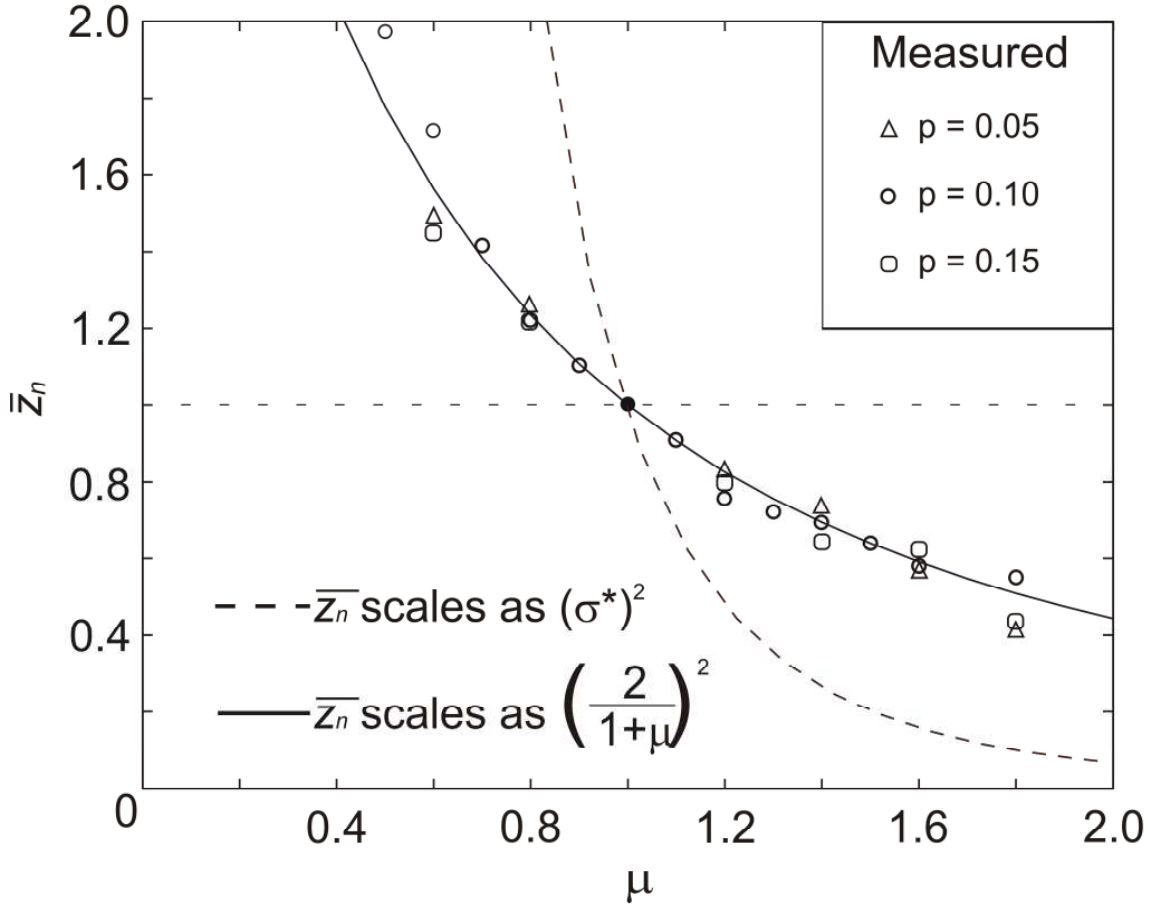


Figure 2. The variation in $\bar{z}_n = \bar{z}_{sb}(\mu) / \bar{z}_{sb}(\mu = 1)$ as a function of μ as predicted by our phase-field model for $p = 0.05, 0.10$ and 0.15 . The data is shown normalised against $\bar{z}_{sb}(\mu = 1)$ in order to facilitate easy comparison and show that the data follows a single trend with respect to variation of μ . It is well documented (see text) that \bar{z}_{sb} decreases systematically (side-branches get closer to the tip) with increasing growth velocity (Peclet) number. For our simulations $\bar{z}_{sb}(\mu = 1)$ varied between 18.2 ($p = 0.05$) and 13.5 ($p = 0.15$). Also shown are calculated values of \bar{z}_n obtained by substitution of the actual values of σ^* as measured from the phase-field simulations into Equ. (5) [dashed line] and the trend obtained if σ^* were varying as $2/(1+\mu)$ [solid line] as predicted by Ref. [15].